Journal of Power Sources 187 (2009) 49–56

Contents lists available at ScienceDirect

Journal of Power Sources

journal homepage: www.elsevier.com/locate/jpowsour

Advances in anodic alumina membranes thin film fuel cell: CsH_2PO_4 pore-filler as proton conductor at room temperature

Patrizia Bocchetta*, Rossella Ferraro, Francesco Di Quarto

Dipartimento di Ingegneria Chimica dei Processi e dei Materiali, Università di Palermo, Viale delle Scienze, 90128 Palermo, Italy

ARTICLE INFO

Article history:
Received 29 May 2008
Received in revised form 8 September 2008
Accepted 19 October 2008
Available online 6 November 2008

Keywords:
Cesium hydrogen phosphate
Anodic alumina membranes
Pore filling
Composite proton conductors
Thin film fuel cell

ABSTRACT

Anodic alumina membranes (AAM) filled with cesium hydrogen phosphate proton conductor have been tested as inorganic composite electrolyte for hydrogen–oxygen thin film ($\leq$50 μm) fuel cell (TFFC) working at low temperatures (25 °C), low humidity (T_{gas} = 25 °C) and low Pt loading (1 mg cm^{-2}). Single module TFFC delivering a peak power of around 15–27 mW cm^{-2}, with open circuit voltage (OCV) of about 0.9 V and short circuit current density in the range 80–160 mA cm^{-2} have been fabricated. At variance with pure solid acid electrolytes showing reproducibility problems due to the scarce mechanical resistance, the presence of porous alumina support allowed to replicate similar fuel cell performances over numerous AAM/CsH_2PO_4 assemblies. A scale-up process of the electrodic area has been optimized in order to increase the delivered peak power of AAM thin film fuel cell. Morphological, chemical and electrochemical studies on the alumina composite electrolyte have been carried out by means of scanning electron microscopy, X-ray diffractometry, Micro-Raman spectroscopy, DTA/DTG analysis, ac impedance spectroscopy and single fuel cell tests.

1. Introduction

Recent advances in solid acid fuel cell (SAFC) have proved the functioning of pure CsH_2PO_4 electrolyte, in both hydrogen and direct methanol fuel cells, by heating the cell temperatures over the superprotonic transition (T_{cell} = 235 °C) through humidity stabilization of the electrolyte (p_{H_2O} = 0.3 atm in the gases) [1–2]. Under atmospheric pressure, the superionic transition of cesium dihydrogen phosphate occurs at temperatures (T_s = 231 °C) very close to the region where the crystal decomposes by dehydration. Thus, a high humidity level inside the fuel cell has been revealed an essential condition in order to favour the superionic transition and avoid the dehydration/decomposition of the salt at high temperatures [3]. At the same time, the high Pt loading and high humidification conditions used in such fuel cells subtract two well known advantages of high temperature fuel cells: the possibility to accelerate the electrode kinetics by using less expensive and lower quantities of catalyst and the absence of humidification equipment control. Moreover, solid acid working over the superprotonic transition are not suitable for cyclic applications (like automobiles), owing to the elevated start-up times requested to reach such high temperatures, together with the use of expensive materials and problems of thermal stress.

The behaviour of solid acid fuel cell at low temperature (down to 25 °C) have not yet been investigated in literature, probably due to the low proton conductivity in solid acid electrolytes (<10^{-6} S cm^{-1} for CsH_2PO_4), the difficulties in the preparation of thin film salt membranes and the possible chemical dissolution of the salt in the water produced at the cathode. In this frame, we have evaluated a possible use of CsH_2PO_4 in room temperature SAFC by embedding with salt highly ordered porous alumina membranes.

In previous works, we have reported a novel method to construct thin film fuel cell, based on the pores filling of 50 μm thick anodic alumina membranes (AAM) with solid proton conductors of different nature [4–5]. The choice of porous anodic alumina is motivated by its unique properties that are promising for fuel cell application:

(1) The extremely ordered porous structure made of parallel cylindrical pores, located into a hexagonally packed arrangement. They can be easily electrochemically grown in a rather wide range of thickness (from few micron to hundreds micron) and porosity (from 10 to 43%) with pores diameter ranging from 20 to 200 nm depending on anodizing parameters through a self-ordering process [6–10]. Thus, through an optimal filling of AAMs, a nanowire-type structure of the proton conductor can

* Corresponding author. Tel.: +39 091 6567233; fax: +39 06 233211963.
E-mail address: bocchetta@dicpm.unipa.it (P. Bocchetta).

0378-7753/$ – see front matter
doi:10.1016/j.jpowsour.2008.10.088

be obtained and a highly precise control of its size (thickness and diameter) should be possible.

(2) Since the polarization curve of solid acid fuel cells [1,4,11] appears mainly controlled by the ohmic drop into the electrolyte, very low membrane thickness should enhance the performance of the fuel cell. The presence of the AAM support could also prevent powdering of the salt and internal short circuit in the cell.
(3) The hydrophilicity of anodic alumina can also contribute to the proton transport at room temperature owing to the presence of water molecules inside the pores.
(4) The easy handling of porous anodic alumina in micromachining operations [12] suggests also a possible realization of novel AAM/solid acid-based micro-fuel cell. If we consider the increasing interest in the development of room temperature fuel cell for customer electronic application, where a significant reduction in weight and size of the power source is required, the integration of AAM in miniaturization processes seems really appealing.

In this paper, it will be shown that the use of a 50-μm highly ordered porous alumina support after impregnation with CsH_2PO_4 allows to fabricate H_2/O_2 room temperature fuel cell with performances comparable to those reported for high temperature CsH_2PO_4 fuel cell, by using low Pt loading and low humidity conditions. Moreover, AAM-based thin film fuel cell generates reproducible power outputs that can be scaled-up by a simple increase of the electrodic area. In spite of the cathodic salt dissolution, the durability at 25 °C of AAM/CsH_2PO_4 MEA has been extended to about 3–4 h, so allowing the use of AAM-based fuel cell in short-time applications (i.e. as possible substitute of thermal batteries in military).

2. Experimental

Commercial (Anodisc-47 Whatman, 0.2 μm) alumina membranes have been employed as support of the proton conductor. The membranes were characterized by pore diameters around 200 nm, porosity of about 43% and thickness of 50 μm. The pore filling of as-received or initially treated membranes was performed with cesium dihydrogen phosphate. The solid acid was synthesized from aqueous solution of Cs_2CO_3 (Aldrich, 99%) and H_3PO_4 (Prolabo, 95%) in stoichiometric ratio and subsequent precipitation inducted by ethanol. Alumina membranes were filled with CsH_2PO_4 salt by wet impregnation or ultrasonic bath of the sample in saturated CsH_2PO_4 aqueous solution for different times. The membranes were subsequently dried by exposure to air for different times and assembled with the electrodes. Pellets of CsH_2PO_4 have been prepared by pressing 5 g of salt at 100 °C and 3 MPa for 3 min.

CsH_2PO_4 as prepared and composite AAM/CsH_2PO_4 membranes were analysed by X-ray diffractometry, performed by a Philips X-Ray Generator (Model PW 1130) and a PW (Model 1050) goniometry. Copper Kα radiation and a scanning rate of 2ϑ 1° min^{-1} was used. The identification was performed according to the JCCD data.

Scanning electron microscopy analysis of AAMs, before and after filling procedure were performed by using a Philips XL30 ESEM Scanning electron microscope, coupled with EDX equipment. Specimen surfaces were sputter coated with gold prior to SEM examination. DTA and TGA analysis was realized on powdered CsH_2PO_4 by using a Netzch STA/409/2 thermal analysis equipment at a heating rate of 5 °C min^{-1}.

The composite membranes prepared were sandwiched between two carbon paper electrodes (Toray 40% wet Proofed-E-Tek), covered with a mixture Pt black/C black (30% Pt on Vulcan XC-72, E-Tek)/CsH_2PO_4 wt 15%, stirred in *n*-butyl acetate for at least 3 h. The catalyst loading was 1 mg cm^{-2} of black platinum. The active area was delimited by insulating silicon rubber having a square hole of 5 and 10 cm^2. The membrane electrode assembly (MEA) was then assembled in a single fuel cell apparatus (FuelCellTechnologies Inc.) and fed with humidified oxygen (99.5% purity, 1 bar), and hydrogen (99.5% purity, 1 bar) at room temperature. Humidification of the anode and cathode gases was done by passing the gases through stainless steel bottles, containing double distilled water. The temperature of the fuel cell, as well as that of the humidifiers was monitored by individual controllers (Electrochem Inc.). The flow rates for the two gases were measured by two flowmeters (Matheson Instruments), placed before the heating bottles. Before recording the polarization curves of the fuel cell, the open circuit voltage was monitored until a quasi-steady-state condition (for 15 min) was reached. Fuel cell tests were performed with composite membranes having different aging times in air, ranging from 1 h to 10 days. Polarization curves were obtained by using a PARSTAT Potentiostat 2263 or an electronic load ARC DL200. A XY chart recorder (HP) was used to record the polarization curves. The current density data reported in the text and figures are referred to the apparent AAM area (5 or 10 cm^2). After each test performed at the fuel cell the MEAs were disassembled in order to verify the integrity of the composite membranes. Preliminary data on conductivity of membranes have been derived by electrochemical impedance spectroscopy with a parstat 2263 potentiostat equipped with an impedance analyser directly connected to the fuel cell. The impedance spectra were recorded in the range 100 kHz to 0.1 Hz at 25 °C and open circuit potential value with an ac amplitude of 10 mV. Before each measurement the fuel cell was stabilized for at least 15 min. Data analysis and equivalent circuit fitting were carried out through a power Suite and a ZSimpleWin softwares. Inductive points acquired at high frequencies were removed.

3. Results and discussion

3.1. Physico-chemical characterizations

The X-ray diffractograms (Fig. 1a and b) recorded for pure cesium dihydrogen phosphate and composite cesium dihydrogen phosphate/porous anodic alumina exhibit the diffraction peaks relative to monoclin CsH_2PO_4 (ICDD Card 35-0746). The salt keeps the same crystalline structure after precipitation inside the amorphous alumina porous structure.

The thermal behaviour of powdered CsH_2PO_4 salt was characterized by thermogravimetry analysis (TG/DTA) conducted in air at a rate of 5 °C min^{-1}. As shown in Fig. 2, the endothermic heat flows at

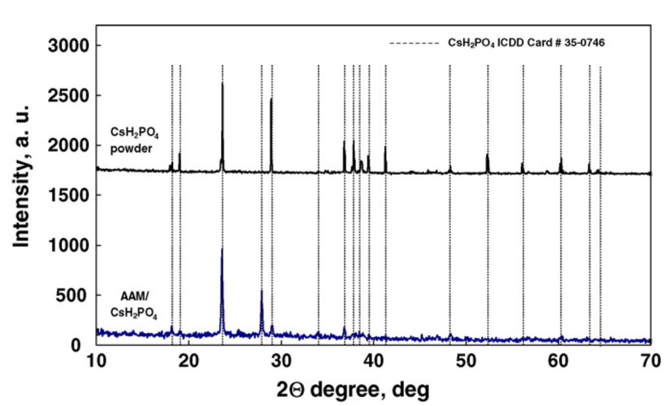

Fig. 1. X-ray diffraction pattern (Cu Kα) recorded at 298 °K for (a) CsH_2PO_4 precipitated as synthesized and (b) anodic alumina membrane after pore filling with CsH_2PO_4.

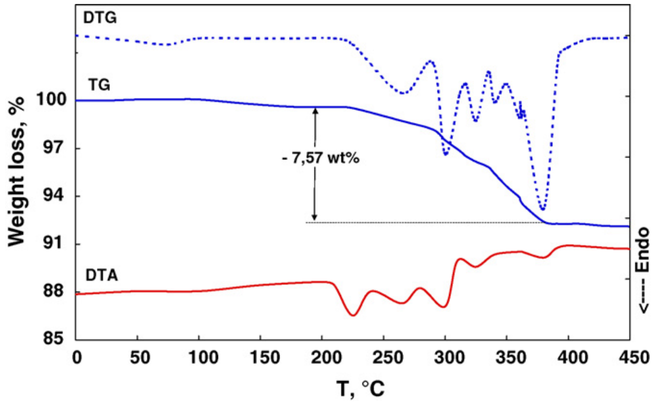

Fig. 2. DTA and DTG curves of CsH_2PO_4 precipitated phase recorded at 5 °C min^{-1} in air.

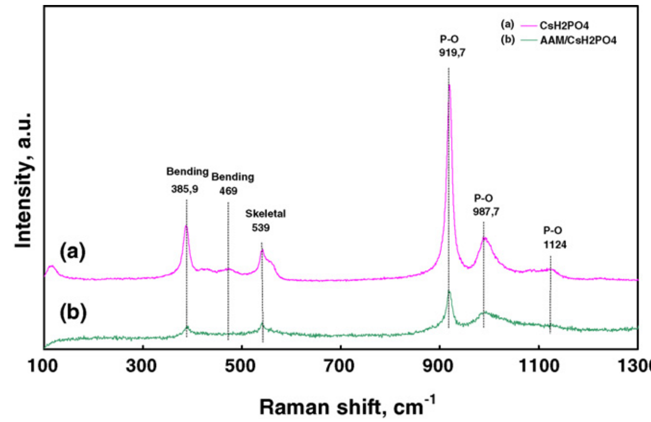

Fig. 3. Micro-Raman spectra of (a) CsH_2PO_4 precipitated as synthesized and (b) anodic alumina membrane after pore filling with CsH_2PO_4.

230 °C is accompanied by the onset of weight loss, suggesting dehydration of CsH_2PO_4. The DTA peak at 230 °C has been reported [13] to be the consequence of thermal decomposition that take place at high temperature in absence of high humidity levels. The polymerization/dehydration process totally suppress the superprotonic transition producing dimeric $Cs_2H_2P_2O_7$ according to

$$2CsH_2PO_4 \rightarrow Cs_2H_2P_2O_7 + H_2O \quad (1)$$

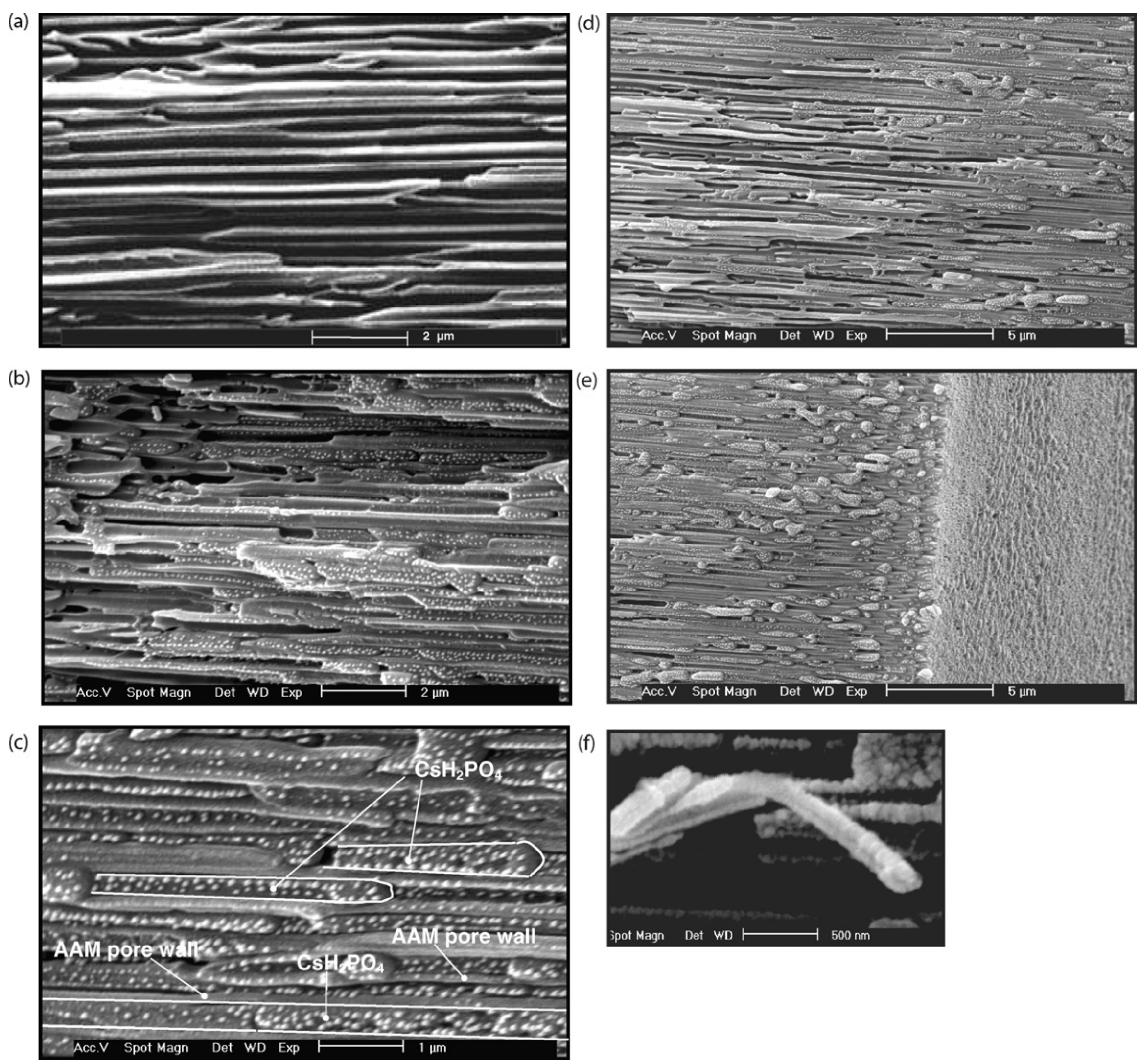

Fig. 4. SEM morphology of pores structure of broken membranes (a) before and (b–e) after filling with CsH_2PO_4 and (f) Particular at higher magnifications evidencing nanorods of CsH_2PO_4.

The DTA peaks (see Fig. 2) at temperatures higher than 230 °C can be attributed to the formation of subsequent polymerization products, described by

$$n\mathrm{CsH_2PO_4} \rightarrow \mathrm{Cs}_n\mathrm{H_2P}_n\mathrm{O}_{3n+1} + (n-1)\mathrm{H_2O}, \qquad n \geq 2 \tag{2}$$

The total weight loss of 7.57% at temperature of 380 °C displayed in Fig. 2 is in agreement with the theoretical value estimated in Ref. [14] for the transformation of CsH_2PO_4 into the final product $CsPO_3$. The TG/DTA analysis relative to the grinded alumina/CsH_2PO_4 samples (not reported), show a lower weight loss (6 wt%) and no DTA peaks above 250 °C, indicating a higher thermal stability of the composite material, which does not complete the polymerization reaction to $CsPO_3$. This is due to the fact that dehydration is a surface modification [15] that cannot be separated from a bulk transformation, such as the superprotonic transition, occurring in the same range of temperatures. Thus, the phenomenon is more enhanced in powdered samples and can be moderated protecting the samples from the surrounding atmosphere [16].

In Fig. 3, Raman spectra of CsH_2PO_4 powder and AAM/CsH_2PO_4 samples are reported. The bands have been assigned to the paraelectric phase (stable at room temperature) of cesium dihydrogen phosphate according the results of Ref. [17]. It is noteworthy that with respect to single crystal, the bands due to the OH^- stretching vibrations in CsH_2PO_4 are usually less visible in polycrystalline samples [18].

3.2. Morphological studies

The informations about the morphology of nano-sized cesium hydrogen phosphate inside the pores of anodic alumina membranes have been obtained by S.E.M. studies carried out on the surfaces and cross-sections of the samples. The structure of the salt is quite similar to that reported for composite AAM/$CsHSO_4$ [4]. Fig. 4a and b shows AAMs side-views before and after filling with CsH_2PO_4. It comes out that the proton conductor fills the cylindrical pores forming wires structures with a good adherence to the inert phase (Al_2O_3) that reduces the gases crossover. The AAM pores walls and the proton conductor are evidenced in Fig. 4c. The particles visible on top of the conductor are probably formed during the high vacuum sample preparation. In Fig. 4d–f, the nanowire-type morphology of CsH_2PO_4 is evidenced. At present, it cannot be discerned if empty pores visible in Fig. 4b, d and e are due to detachment of the acid occurring during the S.E.M. specimens' preparation.

In Fig. 5a, the micrographs of the AAMs surfaces before and after impregnation with CsH_2PO_4 are compared at the same magnification. With respect to composite phosphotungstic acid/AAM and $CsHSO_4$/AAM previously reported in our works [4–5], the proton conductor layer above the alumina surfaces is often absent, as evidenced in Fig. 5b. This result favours better contact between the electrode/electrolyte interfaces and a decrease of the MEA thickness. Assuming that all the solid acid nanowires are continuous along the pores of the AAM, a ratio filled/empty pores of about 80% has been estimated by analysis of SEM pictures similar to that of Fig. 5b.

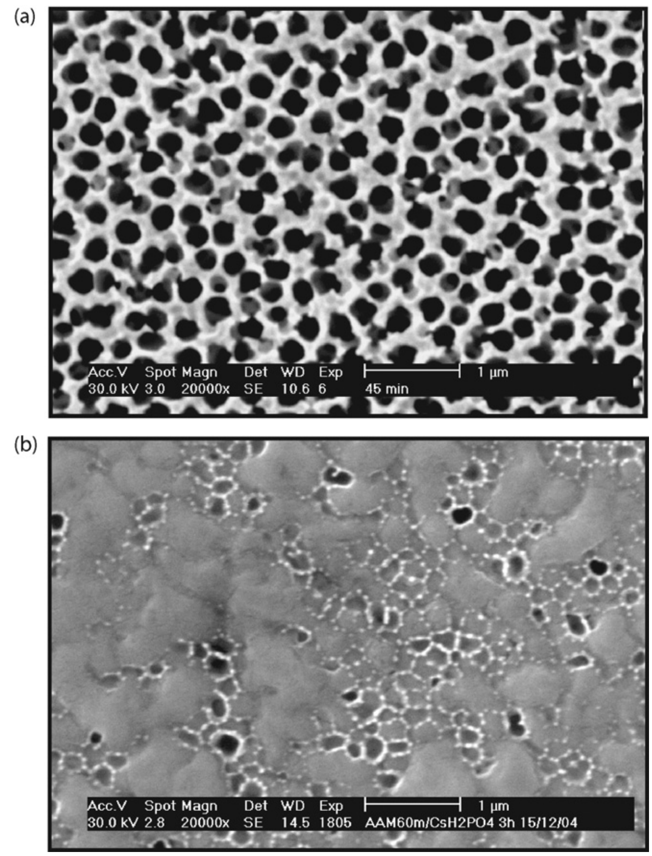

Fig. 5. SEM morphology of the surface of anodic alumina membranes (a) before and (b) after filling with CsH_2PO_4.

3.3. Fuel cell tests

3.3.1. Reproducibility, scale-up and stability of the cell

Before recording the polarization curves of the fuel cell, the open circuit voltage was monitored until a quasi-steady-state voltage was measured (~15 min). The scaling effect of the apparent electrodic area on the power output is shown in Fig. 6, where the average performance of AAM/CsH_2PO_4 electrolyte at 25 °C is reported for: (a) 5 cm^2 and (b) 10 cm^2 single fuel cell module. The deliverable peak power and maximum current increase with the increase of the area by a factor of two, going from 72 to 147 mW, indicating that the scale-up process can be successfully used to meet different needs.

We would like to stress that short circuit current densities (i_{sc}) of about 800 mA and peaks power (P_{max}) of 147 mW have been collected on N. 50 AAM/CsH_2PO_4 assemblies in 10 cm^2 H_2/O_2 single fuel cell apparatus working at room temperature, low humidity (T_{gas} = 25 °C), and low Pt loading (1 mg cm^{-2}). In a few cases, the AAM/CsH_2PO_4 10 cm^2 fuel cell exhibited better performance, as reported in Fig. 7a, where a cell is able to produce short circuit current densities of about 160 mA cm^{-2} and peaks power

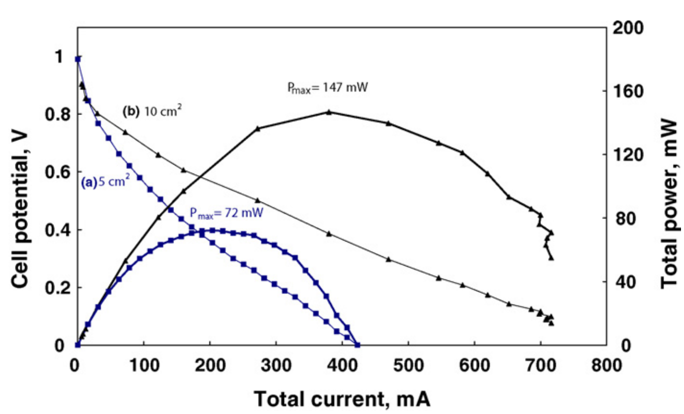

Fig. 6. Polarization curves and power output for (a) 5 cm^2 and (b) 10 cm^2 single module H_2/O_2 fuel cell (T_{cell} = 25 °C, T_{gas} = 25 °C, 1 mg cm^{-2} Pt loading, drying time = 1 h).

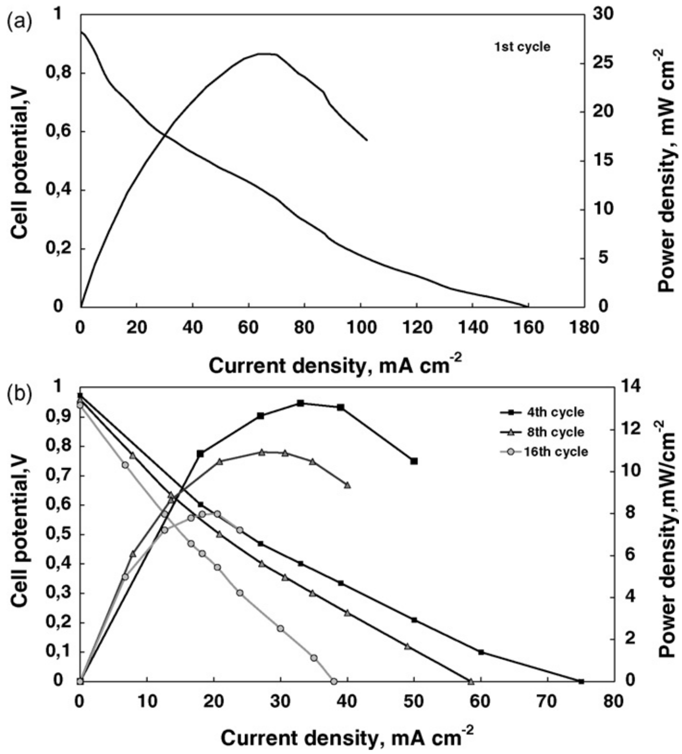

Fig. 7. Best performance for 10 cm^2 single module H_2/O_2 fuel cell (T_{cell} = 25 °C, T_{gas} = 25 °C, 1 mg cm^{-2} Pt loading, drying time = 1 h): (a) 1st cycle and (b) 4th–16th cycle.

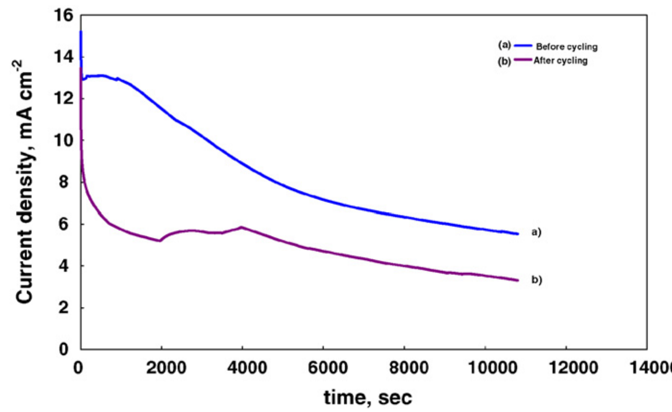

Fig. 8. (a and b) Current output for 10 cm^2 single module H_2/O_2 fuel cell (T_{cell} = 25 °C, T_{gas} = 25 °C, 1 mg cm^{-2} Pt loading, drying time = 1 h) working with AAM/CsH_2PO_4 membranes.

of 27 mW cm^{-2}. These results are encouraging if we consider that the only available literature data relative to room temperature solid acid $Tl_3H(SO4)_2$ fuel cell report very poor performance (i_{sc} = 20–30 μA cm^{-2}) [20]. High-performance solid acid fuel cell electrolytes working at temperature above the superprotonic transition have been extensively studied by the group of Haile and coworkers [1,2,11]. In Ref. [1] pure CsH_2PO_4 electrolyte (260 μm thick) assembled in a H_2/O_2 fuel cell set-up displayed short current density of 0.3 A cm^{-2} and open circuit voltages (OCV) around 1 V at cell temperature of 235 °C, Pt loading of 18 mg cm^{-2} and feeding gas with high humidification (T_{gas} = 80 °C). Our results indicates that high fuel cell performance (i_{sc} = 0.16 A cm^{-2} and OCV around 0.94 V) can be achieved by decreasing the cell temperature to 25 °C and embedding the salt into AAM thin film support, under lower humidity conditions (T_{gas} = 25 °C) and lower Pt loading (1 mg cm^{-2}). We would like to point out that the current and power density reported in this work are relative to the AAM apparent area. Correcting the AAM fuel cell performance for the active area (by assuming the largest measured porosity value of 43%), the short current density and the peak power of TFFC in the best performance of Fig. 7a increase to 0.37 A cm^{-2} and 63 mW cm^{-2}, sensibly close to the values obtained for pure CsH_2PO_4 electrolyte at 235 °C. However, a second aspect to mention is the minor lifetime of our fuel cell with respect to that of Ref. [1]. The performance stability of AAM/CsH_2PO_4 fuel cell at 25 °C has been investigated by cycling the cell voltage or by recording the current output at cell voltage of 0.5 V. By cycling the cell voltage from the open to the short circuit values a decrease of cell performance has been detected. The degradation process affects the short circuit current density value, which for the cell of Fig. 7a changes from the initial 160 to 80 mA cm^{-2} after the 4th cycle and to 40 mA cm^{-2} after the 16th cycle (Fig. 7b). The open circuit voltage was much less affected by cycling, remaining around a value of 0.95 V during the experiment.

These findings suggest a possible dissolution effect of the proton conductor in the water produced in the cathodic flow pattern, as observed in the literature [5,20] for phosphotungstic acid containing membranes, with a loss of contact between protonic conductor and electrocatalytic layer.

In order to evaluate the lifetime of the AAM/CsH_2PO_4 fuel cell the current density vs. time has been recorded at a cell voltage of 0.5 V. The stability curve is shown in Fig. 8 before (a) and after (b) cycling the cell between the open and short circuit voltages. The behaviour of TFFC is characterized by a strong decay of the power output in the first seconds of functioning, followed by a wide peak and finally by a slow decay in the performance estimated to be in the order of 1 μW s^{-1}. In spite of the salt dissolution, the alumina support is able to sustain the cell functioning for at least 3 h.

These experiments indicate that an excess of water influences the stability of the fuel cell, suggesting that an improvement of performance and durability is expected by a better water management in the fuel cell system. A support to this hypothesis comes out from the influence of the initial water content of the composite membranes on the stability test. It seems that composite membranes submitted to long drying times before the assembly resulted in a longer fuel cell stability. As shown in Fig. 9, for drying times of 1 h after the potentiostatic stability test a strong short circuit current density loss to 46 mA cm^{-2} occurs at the first cycle. By continuing cycling further decrease of i_{sc} to 23 mA cm^{-2} is recorded at the 5th cycle.

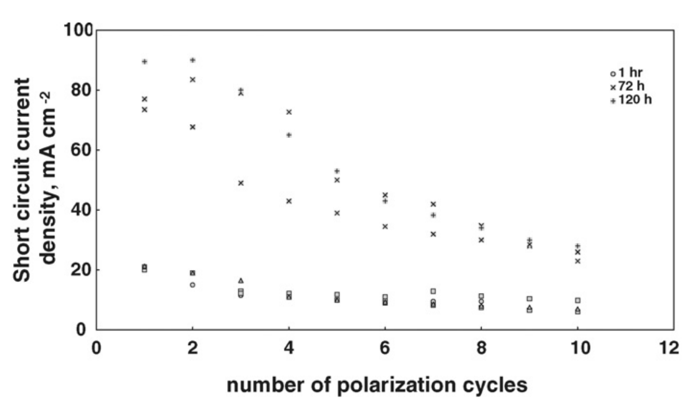

Fig. 9. Short circuit current density (i_{cc}) after the stability test (U_{cell} = 0.5 V for 3 h) reported as reported as function of the number of polarization cycles for a 10 cm^2 single module H_2/O_2 fuel cell (T_{cell} = 25 °C, T_{gas} = 25 °C, 1 mg cm^{-2} Pt loading) working with AAM/CsH_2PO_4 membranes dried for different times (1–120 h).

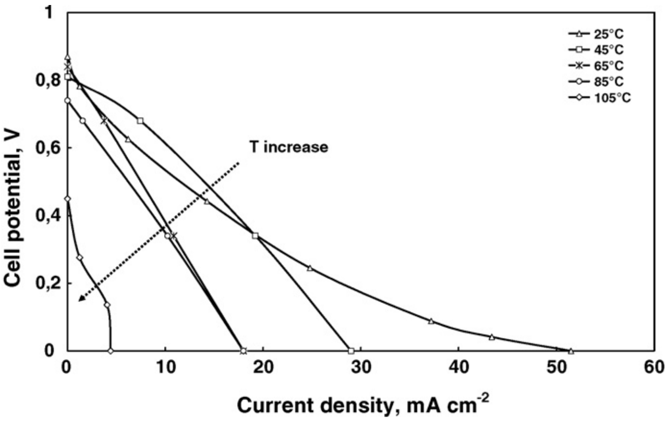

Fig. 10. Polarization curves for a 10 cm^2 single module H_2/O_2 fuel cell working with 50 μm AAM/CsH_2PO_4 membranes dried for 1 h and 1 mg cm^{-2} Pt loading working at different cell temperatures ($T_{gas} = T_{cell}$).

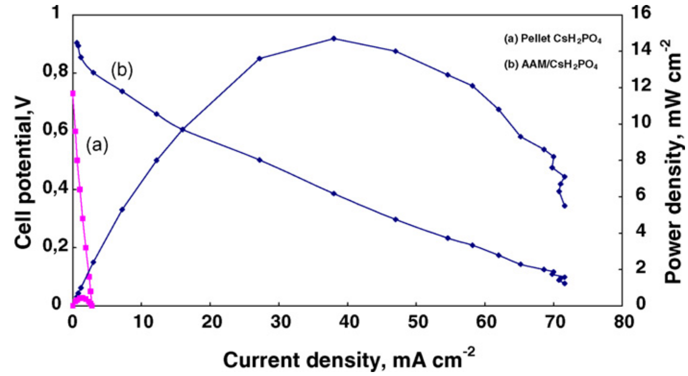

Fig. 11. Polarization curves and power density for a 10 cm^2 single module H_2/O_2 fuel cell (T_{cell} = 25 °C, T_{gas} = 25 °C, 1 mg cm^{-2} Pt loading) working with: (a) 1 mm CsH_2PO_4 pellet and (b) 50 μm AAM/CsH_2PO_4 membranes dried for 1 h.

For AAM/CsH_2PO_4 membranes dried in air for 3–5 days, high performance have been obtained also after stability tests at 0.5 V for 3 h (i_{sc} = 80–90 mA cm^{-2} and P_p = 15–18 mW cm^{-2}). The influence of cycling is reported in Fig. 9, where a slow decay in short current density can be observed, reaching 30 mA cm^{-2} only at the 10th cycle.

3.3.2. *Effect of the cell temperature*

Plots of measured fuel cell performance as a function of the cell temperature (Fig. 10) show an evident decrease with increasing temperature. We assist to a reduction both of the short circuit current density and open circuit potential. The open circuit potential reach the value of zero at cell temperatures in the range 80–120 °C and the short circuit density decrease of one order of magnitude by increasing the cell temperature from 25 to 100 °C. Both OCV and i_{sc} does not recover its initial value during the cell cooling, indicating an increased crossover and ohmic drop into the membrane. The first effect could be attributed to the increased solubility of CsH_2PO_4 in the water produced at the cathode, which leaves an increased unfilled number of pores. The second effect could be attributed to a decrease in the amount of crystallized water inside the proton conductor with consequent reduction of proton mobility. A conductivity decrease with temperature for pure CsH_2PO_4 has been also reported in the work of Otomo et al. [21].

3.3.3. *Effect of the AAM support and proton conductivity at room temperature*

In order to evaluate the effect of the porous alumina support on the fuel cell performance, CsH_2PO_4 pellet of about 1 mm thick have been assembled and tested in the fuel cell. In Fig. 11a and b the cell voltages and the power output as a function of current density are compared for CsH_2PO_4 pellet (a) and CsH_2PO_4/AAM (b) working in a 25 °C H_2/O_2 fuel cell. These data indicate that the alumina succeeds to support thin film CsH_2PO_4, improving the 25 °C fuel cell power output of at least of 1 order of magnitude, passing from 1 to 15 mW cm^{-2} (and to 27 mW cm^{-2} for the best curve of Fig. 7a) by thinning the salt from 1 mm to 50 μm. The preparation of thin film of pure CsH_2PO_4 electrolyte is rather difficult due to the scarce mechanical strength of the salt, giving inevitable reproducibility problems with frequent short circuits between the electrodes. Up to now, thin film (25 μm) CsH_2PO_4 SAFC have been realized and tested in a fuel cell at 240 °C [2], where only four runs are showed and poor mechanical integrity of the electrolyte is evidenced. The thin film MEA of such work must be also mechanically supported with stainless steel electrodes, by hindering its use in miniaturized systems. In this frame, the use of porous alumina seems to be an appealing approach to reduce the electrolyte thickness and enhance the fuel cell output with a good reproducibility and no failures. Some small variations in the power output can be attributed to the catalyst deposition on the electrode, membrane filling technique and time/conditions of AAM/CsH_2PO_4 drying.

An estimation of ionic conductivity has been performed by fitting the ohmic part of the fuel cell polarization curve at 25 °C for pure and AAM-embedded CsH_2PO_4. By assuming that the ohmic drop contributions coming from the cell connections and the electrodes are negligible, membrane resistance values in the range 3–19 and 280 Ω cm^2 are obtained for composite AAM/CsH_2PO_4 and pure CsH_2PO_4, respectively. Normalizing the data with respect to the thickness (50 μm) and the porosity of AAM (43%), conductivity values at 25 °C in the order of (0.6–5) × 10^{-3} and 10^{-4} S cm^{-1} for both AAM/CsH_2PO_4 and pure CsH_2PO_4 have been calculated.

These results have been confirmed by in situ ac impedance measurements conducted in the fuel cell fed with H_2/O_2 at 25 °C and open circuit potential conditions. The Cole–Cole plots for both AAM/CsH_2PO_4 and CsH_2PO_4 fuel cell are reported in Fig. 12. The spectra have been interpreted according to a simple equivalent circuit model, where the membrane electric properties are modelled through a R_mC_m parallel in the high frequencies range and the reaction interfaces are merged into an ideal single interface (parallel of the series R_{ct} W and C_{dl}). Using the membrane resistance values (R_m) obtained from the equivalent circuit fit, proton conductivities have been estimated using the following formula:

$$\sigma = \frac{L}{R_m A}$$

where σ is the conductivity, L is the membrane thickness, A is the electrode area and R_m is the membrane resistance. For the AAM/CsH_2PO_4 membrane the electrode area has been corrected for the AAM porosity (43%). This method yields for AAM/CsH_2PO_4 and pure CsH_2PO_4 ac ionic conductivities in the range 2.6–7.7 × 10^{-3} and 1.8–5.3 × 10^{-4} S cm^{-1}, respectively. The AAM/CsH_2PO_4 ac conductivity data has been also confirmed by impedance analysis in H_2/H_2 symmetrical fuel cell mode (σ = 1.7–2.9 × 10^{-3} S cm^{-1}).

These numbers are sensibly higher with respect to the conductivity values of 10^{-8} S cm^{-1} reported in literature for CsH_2PO_4 single crystal at 80 °C [22]. According to this, we believe that some water present inside the electrolyte could be involved in the mobility of the proton increasing the conductivity of the salt. This suggestion is consistent with the results reported in Ref. [23], where the conductivity of polycrystalline and single crystal CsH_2PO_4 in dry atmosphere were reported to be 10^{-5} and 10^{-8} S cm^{-1} at 100 °C, respectively. The authors investigate the

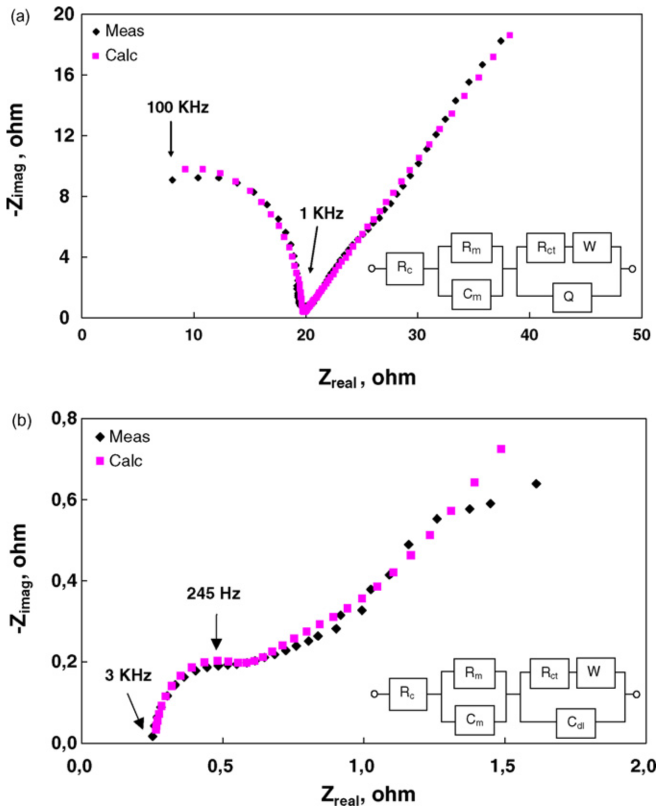

Fig. 12. Ac impedance spectra for a 5 cm^2 single module fuel cell fed with H_2/O_2 at the open circuit potential (T_{cell} = 25 °C, T_{gas} = 25 °C, 1 mg cm^{-2} Pt loading): (a) 1 mm CsH_2PO_4 pellet and (b) 50 μm AAM/CsH_2PO_4 membranes dried for 1 h. Circuit symbols: R_c = circuit resistance; R_m = membrane resistance; C_m = membrane capacitance; R_{ct} = charge transfer resistance; C_{dl} = double layer capacitance; Q = double layer constant phase element; W = Warburg element.

nature of such differences by impedance measurements and found that the apparent highest conductivity of polycrystalline CsH_2PO_4 with respect to single crystalline at low temperatures can be justified by the presence of chemisorbed H_2O in the grain boundary, absent in the single-crystal samples. This behaviour is similar to compounds like $Zr(HPO_4)_2$, a known solid acid material with proton transport dependent from humidity [24]. In addition, the improved conductivity of composite AAM/CsH_2PO_4 with respect to pure CsH_2PO_4 electrolyte suggests a possible contribute of alumina support to the overall proton conductivity. The composite AAM/solid acid of this work seems to behave like solid acid composites prepared by mechanically grinding with porous silica, such as $CsHSO_4$–SiO_2 [25–27] and CsH_2PO_4–SiO_2 [27], which show higher conductivity with respect to pure solid acid at temperature lower than the superprotonic transition. Recently, heterogeneous dispersion of nanoparticles of different oxide phases (such as Al_2O_3, SiO_2, etc.) has become a popular technique of solid-state proton conductors' (ionic salts) modifications [13–29]. Different theories have been made about the enhancement of ionic conductivity in such composites, the more accepted proposing the creation of a modified solid–solid interface (defects source) between the two materials [30–31]. In our electrolytes made of alumina pores filled with CsH_2PO_4 a contribute to the proton conductivity can arise from the hydrophilicity of alumina, which can favour the formation of a H_2O continuous path at the oxide/salt interface promoting the proton hopping through the Grotthüss mechanism [32–33]. Preliminary results obtained from ex situ two-probe impedance spectroscopy at ambient conditions suggest possible role of alumina in the proton transport strictly related to the water balance inside the fuel cell (self-humidifying effect).

4. Conclusions

A new possibility for cesium dihydrogen phosphate fuel cell has been opened by using anodic alumina membranes as thin film support. It has been shown that H_2/O_2 CsH_2PO_4 AAM-based fuel cell can produce high power output (short circuit current densities of 160 mA cm^{-2} and peaks power of 27 mW cm^{-2}) also at room temperature, 1 mg cm^{-2} platinum load and low humidity level, which are less drastic conditions than those typically used in solid acid fuel cell [1,11]. Despite the low thickness of the salt (50 μm), the AAM support guarantees the fuel cell performance with good reproducibility without any external support. The power output of the AAM/CsH_2PO_4 fuel cell system can be enhanced through a simple scale-up process, as demonstrated by the results obtained with two different electrodic areas (5 and 10 cm^2). Moreover, the investigation on MEA in fuel cell single module suggests that the water uptake is a key parameter in regulating the proton conductivity and the stability of the AAM-CsH_2PO_4 electrolyte and opens new challenge in the study of the mechanism of high proton conductivity of a solid acid embedded in a hydrophilic matrix at low temperatures (25 °C). Although the solubility of the salt has not been totally suppressed by the use of alumina membrane, the lifetime of AAM fuel cell has been improved to about 3 h. In conclusion, the AAM-based fuel cell has been improved and optimized with respect to previous works [4–5], indicating that future efforts aimed toward a better water management and/or the use of novel water-insoluble electrolytes could make viable the fabrication of AAM-based thin film fuel cell.

Part of this work has been presented at the Conference 'From physical understanding to novel architectures of fuel cells' held in Miramare, Trieste, Italy (21–25 May 2007).

Acknowledgments

This work is sponsored by US Army-ONRG (USAITC-A under contract N. W911NF-07-1-0564) and Becromal S.p.A. (Milano, Italy). One of the authors (PB) gratefully thanks Regione Sicilia (Program APQ-delibera CIPE n.17/2003) for providing a fellowship.

References

[1] D.A. Boysen, T. Uda, C.R.I. Chisholm, S.M. Haile, Science 303 (2004) 68–70.
[2] T. Uda, S.M. Haile, Electrochem. Solid-State Lett. 8 (2005) A245–A246.
[3] J. Otomo, T. Tamaki, S. Nishida, S. Wang, M. Ogura, T. Kobayashi, C.-J. Wen, H. Nagamoto, H. Takahashi, J. Appl. Electrochem. 35 (2005) 865–870.
[4] P. Bocchetta, G.P. Chiavarotti, R. Masi, C. Sunseri, F. Di Quarto, Electrochem. Commun. 6 (2004) 923–928.
[5] P. Bocchetta, F. Conciauro, F. Di Quarto, J. Solid State Electrochem. 11 (2007) 1253–1261.
[6] R.C. Furneaux, W.R. Rigby, A.P. Davidson, Nature 337 (1989) 147–149.
[7] H. Masuda, K. Fukuda, Science 268 (1995) 1466–1468.
[8] J.W. Diggle, T.C. Downie, C.W. Goulding, Chem. Rev. 69 (1969) 370–397.
[9] G.E. Thompson, Y. Xu, P. Skeldon, K. Shimizu, S.H. Han, G.C. Wood, Philos. Mag. 55 (1987) 651–667.
[10] P. Bocchetta, C. Sunseri, G. Chiavarotti, F. Di Quarto, Electrochim. Acta 48 (2003) 3175–3183.
[11] S.M. Haile, D.A. Boysen, C.R.I. Chisholm, R.B. Merle, Nature 410 (2001) 910–913.
[12] H. Jha, T. Kikuchi, M. Sakairi, H. Takahashi, Appl. Phys. A: Mater. Sci. Process. 88 (2007) 617–622.
[13] J. Otomo, N. Minagawa, C.-J. Wen, K. Eguchi, H. Takahashi, Solid State Ionics 156 (2003) 357–369.
[14] J.-H. Park, Phys. Rev. B 69 (054104) (2004) 1–6.
[15] K.S. Lee, J. Phys. Chem. Solids 57 (1996) 333–342.
[16] Y. Luspin, P. Simon, Solid State Commun. 1188 (2001) 189–193.
[17] F. Romain, A. Novak, J. Mol. Struct. 263 (1991) 69–74.
[18] B. Marchon, A. Novak, J. Chem. Phys. 78 (1983) 2105–2120.
[19] Y. Matsuo, K. Saito, H. Kawashima, S. Ikehata, Solid State Commun. 130 (2004) 411–414.

[20] Y.S. Kim, F. Wang, M. Hickner, T.A. Zawodzinski, J.E. McGrath, J. Membr. Sci. 212 (2003) 263–282.
[21] J. Otomo, T. Tamaki, S. Nishida, S.Q. Wang, M. Ogura, T. Kobayashi, C.J. Wen, H. Nagamoto, H. Takahashi, J. Appl. Electrochem. 35 (2005) 865–870.
[22] E. Ortiz, R.A. Vargas, B.-E. Mellander, Solid State Ionics 125 (1999) 177–185.
[23] D.A. Boysen, S.M. Haile, Chem. Mater. 15 (2003) 727–736.
[24] G. Alberti, M. Casciola, U. Costantino, R. Radi, Gazz. Chim. Ital. 109 (1979) 421–426.
[25] V.G. Ponomareva, N.F. Uvarov, G.V. Lavrova, E.F. Hairetdinov, Solid State Ionics 90 (1996) 161–166.
[26] V.G. Ponomareva, G.V. Lavrova, L.G. Simonova, Solid State Ionics 118 (1999) 317–323.
[27] H. Shigeoka, J. Otomo, C.-Y. Wen, M. Ogura, H. Takahashia, J. Electrochem. Soc. 151 (2004) J76–J83.
[28] A.B. Yaroslavtsev, V.Y. Kotov, Russ. Chem. Bull. 51 (2002) 555–568.
[29] A.B. Yaroslavtsev, Solid State Ionics 176 (2005) 2935–2940.
[30] N.F. Uvarov, P. Vaněk, J. Mater. Synth. Process. 8 (2000) 319–326.
[31] J. Majer, Solid State Ionics 131 (2000) 13–22.
[32] E.C. Dickey, O.K. Varghese, K.G. Ong, D. Gong, M. Paulose, C.A. Grimes, Sensors 2 (2002) 91–110.
[33] S. Walbran, A.A. Kornyshev, J. Chem. Phys. 114 (2001) 10039–10048.